THE JOURNAL OF PHYSICAL CHEMISTRY B

Article

pubs.acs.org/JPCB

Effect of Bisecting GlcNAc and Core Fucosylation on Conformational Properties of Biantennary Complex-Type N-Glycans in Solution

Wataru Nishima,[†] Naoyuki Miyashita,[‡] Yoshiki Yamaguchi,[†] Yuji Sugita,*[,†,‡,§] and Suyong Re*[,†]

[†]RIKEN Advanced Science Institute, 2-1 Hirosawa, Wako, Saitama 351-0198, Japan

[‡]RIKEN Quantitative Biology Center, IMDA 6F, 1-6-5 Minatojimaminamimachi, Chuo-ku, Kobe, Hyogo 650-0047, Japan

[§]RIKEN Advanced Institute for Computational Science, 7-1-26 Minatojimaminamimachi, Chuo-ku, Kobe, Hyogo 650-0047, Japan

Supporting Information

ABSTRACT: The introduction of bisecting GlcNAc and core fucosylation in N-glycans is essential for fine functional regulation of glycoproteins. In this paper, the effect of these modifications on the conformational properties of N-glycans is examined at the atomic level by performing replica-exchange molecular dynamics (REMD) simulations. We simulate four biantennary complex-type N-glycans, namely, unmodified, two single-substituted with either bisecting GlcNAc or core fucose, and disubstituted forms. By using REMD as an enhanced sampling technique, five distinct conformers in solution, each of which is characterized by its local orientation of the Manα1-6Man glycosidic linkage, are observed for all four N-glycans. The chemical modifications significantly change their conformational equilibria. The number of major conformers is reduced from five to two and from five to four upon the introduction of bisecting GlcNAc and core fucosylation, respectively. The population change is attributed to specific inter-residue hydrogen bonds, including water-mediated ones. The experimental NMR data, including nuclear Overhauser enhancement and scalar *J*-coupling constants, are well reproduced taking the multiple conformers into account. Our structural model supports the concept of "conformer selection", which emphasizes the conformational flexibility of N-glycans in protein−glycan interactions.

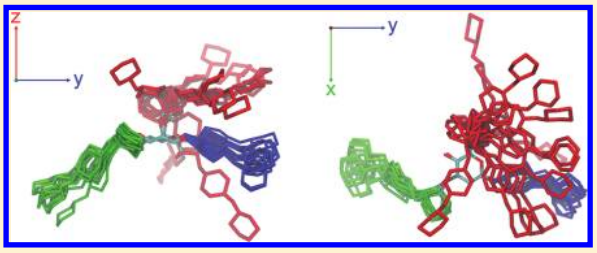

INTRODUCTION

The N-linked oligosaccharides (N-glycans) participate in various biological functions including folding control,[1] cell adhesion,[2] and immune response.[3] Modifications of N-glycans, for example, through the introduction of bisecting GlcNAc and/or core fucosylation, are known to modulate the function and regulation of the particular proteins involved.[4] The addition of bisecting GlcNAc by GlcNAc transferase III (GnT-III) to the cell adhesion molecules, E-cadherin and integrins, suppresses cell migration.[5] The introduction of bisecting GlcNAc into cell surface receptors, such as the epidermal growth factor receptor (EGFR), contributes to the suppression of metastasis.[5] It is well characterized that addition of bisecting GlcNAc inhibits further oligosaccharide maturation by enzymes such as GnT-V.[5] On the other hand, antibodies lacking core fucose show greatly increased affinity to the Fcγ receptor, thereby improving antibody-dependent cellular cytotoxicity.[6] The mechanism underlying such modification-induced changes in N-glycan−receptor interactions remains unclear. The concept of conformer selection upon binding (selection of a particular "key" from a "bunch of keys"[7]) is widely accepted as the basis for glycan−receptor interactions.[8,9] Generally, glycan consists of rigid saccharide units linked together through flexible glycosidic bonds, giving rise to the possibility of multiple conformers in solution. A different conformer could bind to a different receptor. For example, both cholera toxin and galectin-1 bind to the pentasaccharide of ganglioside GM1 but each to a different conformer.[10] The introduction of bisecting GlcNAc and/or core fucosylation could change binding, by way of either switching the major conformation from one to another or inducing a unique bioactive conformation, rather than by making an additional unique binding site.

Past structural studies on N-glycans show the importance of conformational diversity for glycan−receptor interactions.[11] A survey of crystallographic data on oligosaccharide structures reveals several distinct conformers for local glycosidic linkages, particularly for Manα1-6Man.[11,12] Due to the inherent flexibility of N-glycans, high-resolution X-ray structures are available only for receptor-bound N-glycans. Therefore, NMR spectroscopy has been extensively used to analyze solution conformations of N-glycans[13−17] including receptor-bound states.[18,19] The glycan chain is known to undergo a conformational transition between "folded" and "extended" forms. A systematic NMR-based analysis of biantennary N-glycans[13] suggests that bisecting GlcNAc not only restricts the conformational flexibility of the Manα1-6Man linkage[15] but also induces

Special Issue: Macromolecular Systems Understood through Multi-scale and Enhanced Sampling Techniques

Received: December 28, 2011
Revised: April 10, 2012
Published: April 24, 2012

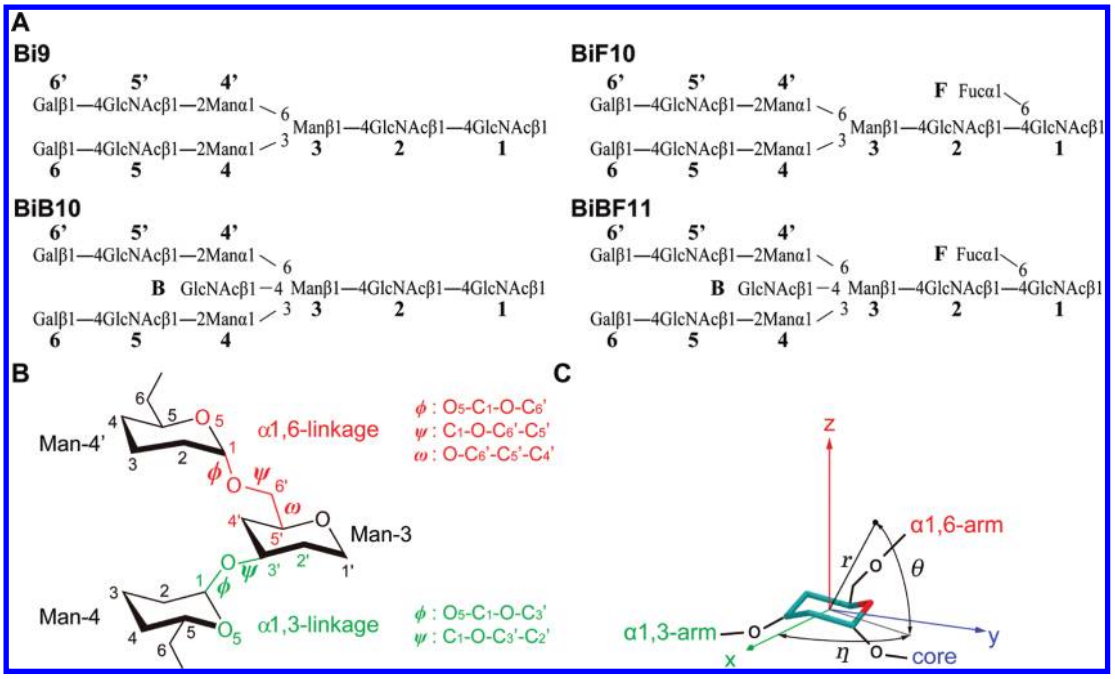

Figure 1. (A) Schematic representation of the four biantennary complex-type N-glycans. Bi9: unmodified, BiB10: single substitution with bisecting GlcNAc, BiF10: single substitution with core-fucose, BiBF11: disubstitution with bisecting GlcNAc and core-fucose. The residues from 1 to 3, from 4 to 6, and from 4′ to 6′ comprise the core, α1,3-arm, and α1,6-arm, respectively. (B) Definition of three dihedral angles, ϕ, ψ, and ω, for α1,6-linkage and two dihedral angles, ϕ and ψ, for α1,3-linkage. (C) Definition of the spherical coordinate. The angle η represents *swing* motion of the α1,6-arm around the z (polar) axis, while the angle θ represents *up down* motion with respect to the xy-plane (see text for details).

a unique Manα1-3Man conformation.[14] The same analysis also suggests that core fucosylation does not cause such changes.[13] NMR spectroscopy provides the structure and dynamics of the local glycosidic linkages but is limited in probing the overall motion of the glycan antennae in solution. As regards the latter, fluorescence resonance energy transfer (FRET) has been used and shows a significant effect of the core fucose on the ratio of the "folded/extended" populations.[20]

Molecular dynamics (MD) simulation provides insights into structural and dynamic aspects of N-glycans in atomic detail not normally accessible by experiment.[16,21−34] MD simulations applied to biantennary N-glycans in solution predict that the introduction of the bisecting GlcNAc and/or core fucosylation induce a conformational transition between "folded" and "extended" forms.[28] However, past conventional MD simulations in explicit solvent have been limited to small fragments like mono-, di-, or trisaccharides,[16,21−25] or larger fragments with short sampling.[26−28] In previous work, we employed replica-exchange molecular dynamics (REMD)[35] to fully characterize the multiple conformers of biantennary complex-type N-glycans in solution.[36] Our simulations, with extensive sampling of N-glycan structures in solution, revealed five distinct conformers for the N-glycan rather than the two ("extended" and "folded" forms) previously discerned. The results clearly show that the introduction of bisecting GlcNAc reduces the conformational variety, signifying the importance of "conformer selection"[8,9] for fine regulation of the binding affinity to the target protein. Here, we follow up on this work with core fucosylation, another important N-glycan modification, to provide a comprehensive model of the structures. The model provides insight into the changes in conformational equilibria of the N-glycan in solution in terms of global structures, local glycosidic linkages, and underlying hydrogen-bond (H-bond) interactions.

METHODS

REMD simulations were carried out using an in-house interface program (REIN: Replica-Exchange INterface version 0.1).[37] The NAMD program package[38] was used for the MD runs within the interface program. The Glycam_06_G force field parameter[29,39] for oligosaccharides and a TIP3P model[40] for water molecules were used.

We used four biantennary complex-type N-glycans, as shown in Figure 1A: the unmodified N-glycan (Bi9), the two species substituted singly with either bisecting GlcNAc (BiB10) or core fucose (BiF10), and the disubstituted form (BiBF11). The simulation results for Bi9 and BiB10 have been reported previously,[36] but we analyzed the trajectories again to obtain a comprehensive picture of the N-glycan modifications. The initial configurations of the four N-glycans were constructed using the GLYCAM web portal (Glycam Biomolecule Builder), www.glycan.com.[41] Each molecule was solvated within a rectangular box containing 3437, 3289, 4677, and 5085 TIP3P water molecules for Bi9, BiB10, BiF10, and BiBF11, respectively. The system was initially equilibrated in a NPT ensemble for 1 ns to determine the system volume at 1 atm. An additional 1 ns MD simulation was carried out in the NVT ensemble to equilibrate the system with box sizes of 47 × 45 × 51, 40 × 48 × 54, 45 × 54 × 60, and 59 × 47 × 57 Å^3 for Bi9, BiB10, BiF10, and BiBF11, respectively. A constant temperature of 300 K was maintained using Langevin dynamics with a damping constant of 5 ps^{-1}. Long-range electrostatic forces were calculated using the smooth particle-mesh Ewald summation method[42] with a grid size of less than 1 Å. A time step of 2 fs was used for the integration. The final snapshots were used for the subsequent REMD simulations. Sixty-four replicas were used to cover the temperature range 300−500 K. Replica exchange was carried out every 2 ps, and each replica simulated for 52 ns. This gives a total simulation

dx.doi.org/10.1021/jp212550z | J. Phys. Chem. B 2012, 116, 8504−8512

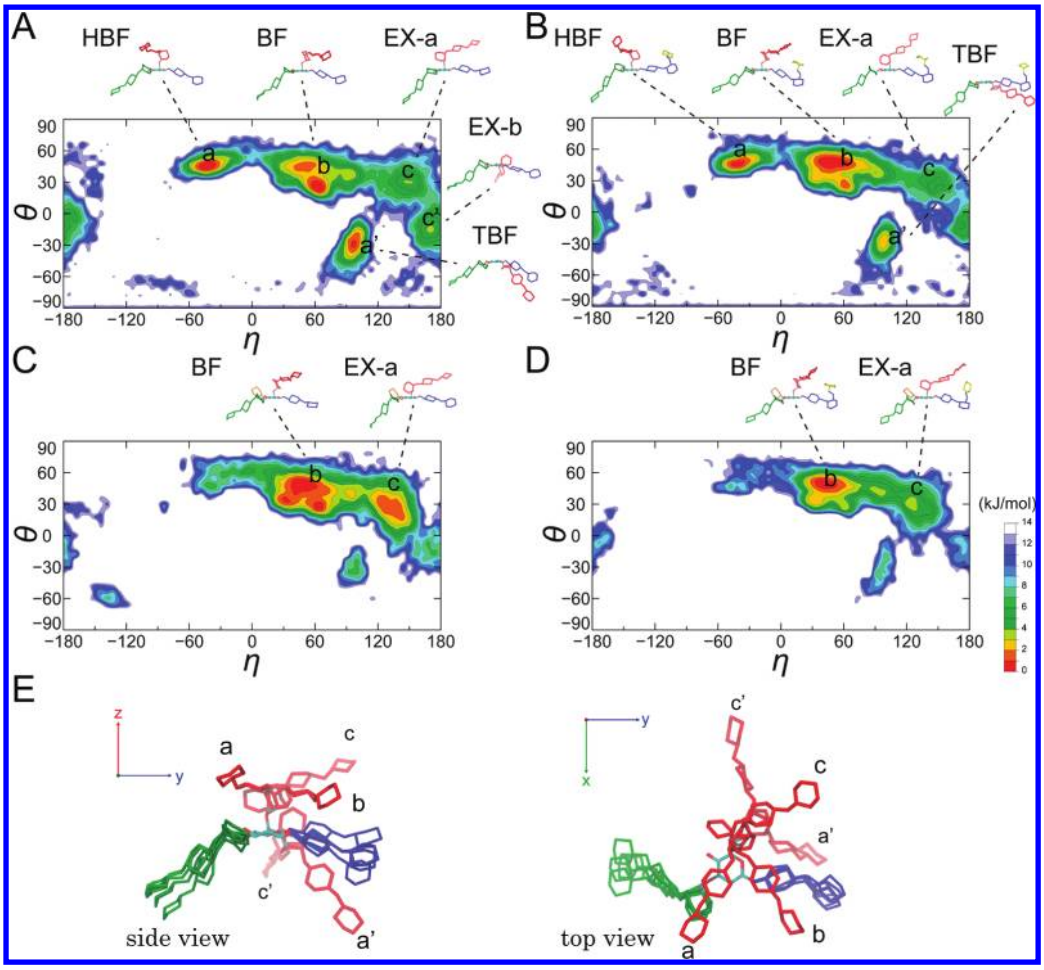

Figure 2. Free-energy maps of global conformations of N-glycans using a spherical coordinate: (A) Bi9, (B) BiF10, (C) BiB10, and (D) BiBF11. Alphabetic characters on the map represent peak positions for the major conformers listed in Table 1. (E) A collective view of five major conformers (all conformers are superimposed on the Man-3 pyranose ring).

time of 3.3 μs (52 ns × 64 replica = 3328 ns) for each N-glycan system.

The effect of the introduction of bisecting GlcNAc and core fucosylation on N-glycan conformations was analyzed in terms of the orientation of a local glycosidic linkage as well as the global N-glycan structure. We used three glycosidic dihedral angles defined as ϕ = O_5−C_1−O−C_6', ψ = C_1−O−C_6'−C_5', and ω = O−C_6'−C_5'−C_4' for the Manα1-6Man linkage and two dihedral angles defined as ϕ = O_5−C_1−O−C_3' and ψ = C_1−O−C_3'−C_2' for the Manα1-3Man linkage (Figure 1B). The global structure was represented using a spherical coordinate, as shown in Figure 1C. First, an average structure of Man-3 was made using all the simulation snapshots fitted to the reference (initial) structure. Next, the average structure was aligned with a hexagon on the *xy* plane, with its center at the origin. Finally, the Man-3 structure of each simulation snapshot was superimposed on the average structure on the *xy* plane. This procedure allowed us to determine a unique orientation of the N-glycan global structure with respect to the Man-3 structure, by reducing the artificial orientation changes arising from distortion of the pyranose ring in the simulation snapshots. The axis perpendicular to the hexagon plane was defined as the *z* (polar) axis. The *x* (azimuth) axis was defined as the axis that passes the origin and a vertex of the hexagon corresponding to the C2 atom of Man-3. The distance between the origin and the C1 atom of Gal in the α1,6-arm was defined as the radius, *r*. The azimuthal angle, η, is the angle between the *x* (azimuth) axis and the orthogonal projection of the vector *r* on the *xy*-plane. The polar angle, θ, is the angle measured from the *xy*-plane to the vector *r*. In the previous study, we drew an end-to-end distance free-energy map for the analysis.[36] The present coordinates are found to better represent the relation between the local orientation of the glycosidic linkage and the global structure of the N-glycan.

To validate our simulations, scalar ^3J-coupling constants and nuclear Overhauser enhancement (NOE) distances were calculated from the MD simulation. Scalar *J*-coupling constants were calculated using the modified Karplus equation of Altona and Haasnoot:[43]

$$^3J_{HH} = P_1 \cos^2\phi - P_2 \cos\phi + P_3 + \sum_i \Delta\chi_i\{P_4 + P_5 \cos^2(\xi_i\phi + P_6|\Delta\chi_i|)\}$$

where the suffix *i* indicates the number of substituents attached to the H−C−C−H fragment (i = 3 in the present case), P_1−P_6 are empirically determined parameters (13.22, −0.99, 0, 0.87, −2.46, and 19.90), $\Delta\chi_i$ is the electronegativity ($\chi_i - \chi_{hydrogen}$) of each substituent attached to the H−C−C−H fragment (1.30 for i = 1 and 2 and 0.40 for i = 3), and ξ_i is the orientation of the substituents at the two carbon atoms of the H−C−C−H fragment (ξ_1 = −1 and ξ_2 = ξ_3 = 1 for J_{56}, ξ_1 = ξ_2 = −1 and ξ_3 =

dx.doi.org/10.1021/jp212550z | J. Phys. Chem. B 2012, 116, 8504−8512

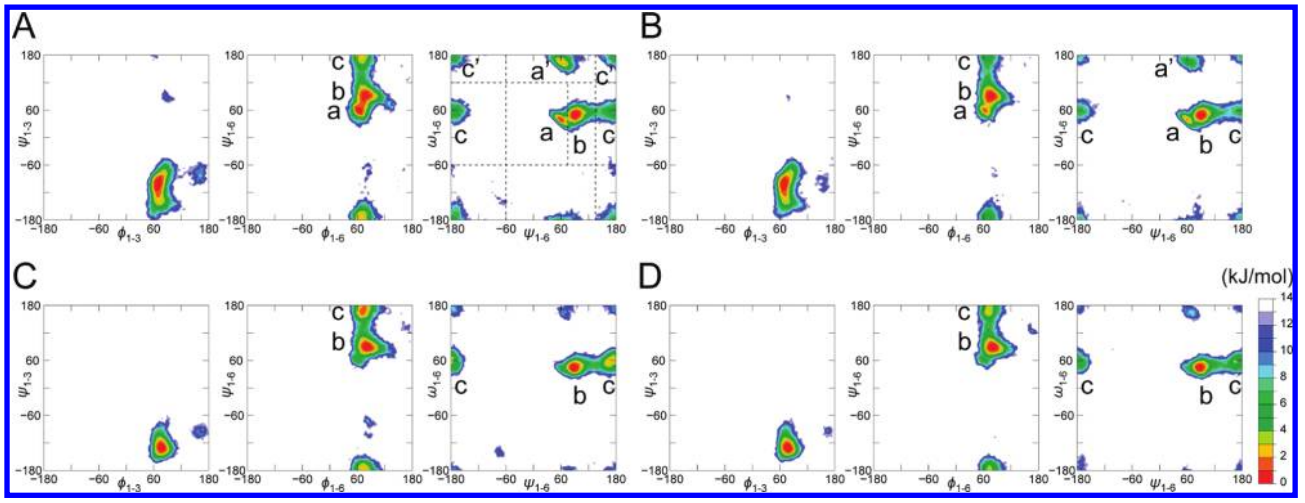

Figure 3. Free-energy maps of dihedral angles ϕ, ψ, and ω for Manα1-3Man and Manα1-6Man: (A) Bi9, (B) BiF10, (C) BiB10, and (D) BiBF11. The dashed line indicates the separation of ψ/ω space used for the calculation of the population size of each conformer. Alphabetic characters on the map represent peak positions for the major conformers in Figure 2 and Table 1.

1 for $J_{56'}$). The coupling constants were calculated for three clusters with different ω orientations ($0° \le \omega < 120°$ (gauche−gauche), $120° \le \omega < 180°$ and $-180° \le \omega < -120°$ (gauche−trans), and $-120° \le \omega < 0°$ (trans−gauche)), and their weighted averages compared with those derived from actual experiments.

$$^3J_{HH} = c_{gg}\,^3J^{gg}_{HH} + c_{gt}\,^3J^{gt}_{HH} + c_{tg}\,^3J^{tg}_{HH}$$

where c_{gg}, c_{gt}, and c_{tg} are the weights for each cluster of gg, gt, and tg conformers. NOE distances were calculated as[44]

$$\frac{1}{r^6_{MD}} = \frac{c_a}{\langle r^6_a\rangle} + \frac{c_b}{\langle r^6_b\rangle} + \frac{c_c}{\langle r^6_c\rangle} + \frac{c_{a'}}{\langle r^6_{a'}\rangle} + \frac{c_{c'}}{\langle r^6_{c'}\rangle}$$

where r_a−$r_{c'}$ are the proton−proton distances for the a−c′ conformational clusters and c_a−$c_{c'}$ represent the weights for each cluster, respectively.

RESULTS AND DISCUSSION

Performance of REMD Simulations. Here we examine whether the temperatures are optimally distributed and the number of replicas sufficient. The acceptance ratios of replica exchange corresponding to the adjacent pairs of temperature are almost constant around 48.5% in the simulation of Bi9, implying a free random walk in the replica (temperature) space (Figure S1A in the Supporting Information). We confirm a free random walk both in the replica space (Figure S1C, Supporting Information) and the temperature space (Figure S1B, Supporting Information). For instance, replica 1, which starts at 300 K, reached the highest temperature (500 K) three times during 52 ns of simulation. The canonical probability distribution of total potential energy at each temperature has sufficient overlap with those of neighbors (Figure S1D, Supporting Information). The REMD simulations of the other N-glycans, BiB10, BiF10, and BiBF11, performed similarly. The average acceptance ratios were 49.5, 41.7, and 39.8% for BiB10, BiF10, and BiBF11, respectively. These results guarantee simulation reliability.

Global N-Glycan Conformation. The present REMD simulations show a variety of conformations of the N-glycans in solution. Five distinct conformers are observed with BiF10 and BiBF11, as we found previously with Bi9 and BiB10.[36] These conformers are characterized by different orientations of the α1,6-arm. There are no significant structural changes within each arm (α1,3- and α1,6-arms) (see Figure S2, Supporting Information). Figure 2 shows the free-energy maps of the four N-glycan systems using a spherical coordinate (see the Methods section for coordinate definitions; in short, the horizontal axis (η) represents the *swing* motion of the α1,6-arm around the z (polar) axis, while the vertical axis (θ) represents the *up down* motion with respect to the xy-plane). Representative conformers are also shown in the same figure. There are three conformers with positive θ values (**a**, **b**, and **c**). The α1,6-arm interacts with both the core and the α1,3-arm through H-bonds in the "half backfold (HBF)" conformer (**a**, $\eta \sim -60°$), whereas it forms an H-bond only with the core in the "backfold (BF)" conformer (**b**, $\eta \sim 60°$). In the "extend-a (EX-a)" conformer (**c**, $\eta > 120°$), the α1,6-arm is fully solvated and makes no direct contact to the core or the α1,3-arm. Correspondingly, there are two conformers with negative θ values (**a**′ and **c**′). The α1,6-arm has its nonpolar B-face oriented toward the nonpolar face of the core in the "tight backfold (TBF)" conformer (**a**′, $\eta \sim 60°$), whereas it is fully solvated in the "extend-b (EX-b)" conformer (**c**′, $\eta > 120°$). Note that the population of the BF conformer could be divided into three subconformers that have slightly different orientations of the α1,6-arm.

We have previously shown that bisecting GlcNAc suppresses this conformational variety by shifting the relative population size of each conformer.[36] As a result, there are only two major conformers, BF (**b**) and EX-a (**c**), in BiB10 (Figure 2C). A similar population suppression is observed for BiBF11 (Figure 2D). The population size of EX-a (**c**) in BiBF11 is smaller than that of BiB10, indicating that the core fucose interacts with the α1,6-arm to prevent the arm from being fully solvated. In BiF10 (Figure 2B), the effect of the core fucose is smaller than that of the bisecting GlcNAc, leaving four major conformers, three "folded" types (**a**, **b**, and **a**′) and one "extended" (**c**) type. In our simulations, the changes in the orientation of the α1,3-arm were observed as minor events compared with those of the α1,6-arm. This picture differs from that obtained previously in MD simulations of the same glycan systems in solution.[28]

Local α1,3/α1,6-Glycosidic Linkage Conformation. Figure 3 shows free-energy maps for the orientation of the

dx.doi.org/10.1021/jp212550z | J. Phys. Chem. B 2012, 116, 8504−8512

Table 1. Populations of Major Conformers in Bi9, BiB10, BiF10, and BiBF11[a]

			populations (%)				
conformers	ψ	ω	Bi9	BiB10	BiF10	BiBF11	Types
a	60°	60° (gg)	**15**	5	**16**	6	HBF
b	90°	60° (gg)	**41**	**51**	**57**	**61**	BF
c	180°	60° (gg)	**15**	**37**	**12**	**27**	EX-a
a′	60°	180° (gt)	**17**	2	**10**	3	TBF
c′	180°	180° (gt)	**11**	4	6	3	EX-b

[a]Populations: distribution of each conformer having ψ/ω angles in a specific range, **a**: $-60° \le \psi < 75°$ and $-60° \le \omega < 120°$, **b**: $-75° \le \psi < 135°$ and $-60° \le \omega < 120°$, **c**: $(-60 > \psi$ or $135° \le \psi)$ and $-60° \le \omega < 120°$, **a′**: $-60° \le \psi < 135°$ and $(\omega < -60°$ or $120° \le \omega)$, **c′**: $(-60° > \psi$ or $135° \le \psi)$ and $(\omega < -60°$ or $120° \le \omega)$. HBF: "half backfold", TBF: "tight backfold", BF: "backfold", EX-a: "extend-a", EX-b: "extend-b". Bold characters represent populations greater than 10%.

first glycosidic linkages of the α1,3/α1,6-arms in the four N-glycans. The results for Bi9 and BiB10 (Figure 3A and C) have been reported in our previous paper.[36] In brief, the Manα1-3Man linkage adopts a broad conformation with a wide range of ψ angles, whereas there are five distinct conformers each having different ψ (60, 90, and 180°) and ω (60 and 180°) angles in the Manα1-6Man linkage. For the same ψ orientation, the gauche−gauche (gg) conformers (ω = 60°) are more prevalent than the gauche−trans (gt) conformers (ω = 180°), consistent with the NOE data.[27] Three conformers (**a**, **a′**, and **b**) with ψ angles of 60 and 90° dominate over the other two (**c** and **c′**) with ψ angle of 180°. The simulation includes all conformations seen by X-ray crystallography.[11,12]

The introduction of bisecting GlcNAc and core fucose reduces the conformational variety of the Manα1-6Man linkage in BiB10, BiF10, and BiBF11. The two modifications almost invariably reduce the population sizes of the gt conformers (**a′** and **c′**, ω = 180°). In BiB10 (Figure 3C), the population sizes of the two conformers **a** and **a′** (ψ = 60°) also drastically decrease, while that of conformer **c** (ψ = 180°) slightly increases.[36] In BiF10 (Figure 3B), core fucosylation affects the linkage conformation only slightly, leaving four major conformers (**a**, **a′**, **b**, and **c**). The population size of conformer **c** is also slightly reduced in BiF10. The disubstituted form (BiBF11, Figure 3D) has a conformational equilibrium very similar to that of BiB10 (Figure 3C), except that the population size of conformer **c** (ψ = 180°) is decreased. Note that the ψ angle distribution of the Manα1-3Man linkage narrows on introducing the bisecting GlcNAc (Figure 3C), whereas core fucosylation rarely affects its range (Figure 3B).

An issue in structural studies of N-glycans is how the extremely flexible glycosidic linkage relates to global structure.[27] Our results show that the population variation seen in Figure 3 closely relates to the global conformation, as listed in Table 1 (see also Figures S3 and S4, Supporting Information). Each angle (ψ/ω) in the Manα1-6Man linkage is characterized by a unique conformation. The ψ and ω angles correspond to the η (*swing* motion) and θ (*up down* motion) angles in Figure 2, respectively. The ω of 60° (gg) leads to three conformers (**a**, **b**, and **c**) with a positive θ value, whereas the ω of 180° (gt) gives two conformers (**a′** and **c′**) with a negative θ value. In each ω orientation, there are both the "folded" and "extended" types of conformations depending on the ψ value. The ψ angles of 60 and 90° lead to HBF (**a**, 60°/60°), BF (**b**, 90°/60°), and TBF (**a′**, 60°/180°) conformers, whereas the ψ of 180° leads to EX-a (**c**, 180°/60°) and EX-b (**c′**, 180°/180°) conformers. NMR-based analysis has suggested that the introduction of bisecting GlcNAc generates a unique conformation of the α1,3-arm.[14] The present simulations show that the bisecting GlcNAc shifts the minimum position of the Manα1-3Man from φ/ψ of 70°/−90° to 70°/−130°, without affecting the global conformation of the α1,3-arm, contrary to the NMR-based prediction.

Inter-Residue Hydrogen Bonds (H-Bonds). Stabilization of a particular conformer by bisecting GlcNAc and core fucose modifications relies on rearrangement of inter-residue H-bonds. Figure 4 shows the probability distribution of the inter-residue H-bonds found in the simulations of the four N-glycans. A schematic illustration of the inter-residue H-bonds is provided in Figure 5. We adopt the following geometric definition for the H-bond: $R_{XX'} < 3.5$ Å, $\theta_{XHX'} > 120°$, where $R_{XX'}$ is the distance between the donor (X) and acceptor heavy atoms (X′) and $\theta_{XHX'}$ is the angle between the XH and the X′H vectors. Figure 4A shows that each H-bond correlates well with a particular conformation. 6 out of 10 H-bonds involve the substituted residue (bisecting GlcNAc or core fucose) as a donor or an acceptor. In Bi9, four H-bonds are found. Two H-bonds, $4'O_6\cdots 2O_3$ and $6'O_2\cdots 4O_3$, contribute to stabilize the HBF conformer (ψ/ω of 60°/60°). On the other hand, each single H-bond, $5'N_2\cdots 2O_3$ or $5'N_2\cdots 2O_6$, is found in the BF (90°/60°) or TBF conformers (60°/180°), respectively.

The bisecting GlcNAc significantly suppresses the formation of these H-bonds except for the $5'N_2\cdots 2O_3$. Three H-bonds between the bisecting GlcNAc and α1,3-arm residues ($5N_2\cdots BO_{2N}$, $5O_6\cdots BO_3$, and $BO_3\cdots 6O_6$) sterically hinder formation of the $6'O_2\cdots 4O_3$ H-bond. The $BN_2\cdots 4'O_6$ H-bond breaks the $4'O_6\cdots 2O_3$ H-bond. In effect, the $5'N_2$ preferentially forms an H-bond with $2O_3$ as an acceptor. These H-bond rearrangements proximal to the bisecting GlcNAc lead to the increase in the population sizes of both BF and EX-a conformers. The core fucose forms two H-bonds, $2N_2\cdots FO_2$ and $FO_2\cdots 5'O_3$, almost exclusively stabilizing the BF conformer. In the presence of these H-bonds, the $5'N_2\cdots 2O_3$ H-bond frequently stabilizes the BF conformer. This net stabilization of the BF conformer is more pronounced in the disubstituted form (BiBF11). In effect, this reduces the population size of the EX-a form in BiBF11 (Figure 2D). In contrast to the bisecting GlcNAc, the core fucose strengthens existing H-bonds without significantly rearranging them.

Figure 4B shows the probability distribution of the inter-residue H-bonds mediated by a single water molecule. There are four H-bonds that mainly stabilize the BF and EX-a forms. The $5N_2\cdots W\cdots BO_{2N}$ H-bond shows the highest probability. The same residue pair also forms a direct H-bond as shown in Figure 4A. The direct and water mediated H-bonds similarly hold the bisecting GlcNAc and GlcNAc-5 in the α1,3-arm (Figure 6). NMR-based analysis has suggested that this H-bond causes a conformational rearrangement of the α1,3-arm.[14] The present simulation shows that it significantly increases back

dx.doi.org/10.1021/jp212550z | J. Phys. Chem. B 2012, 116, 8504−8512

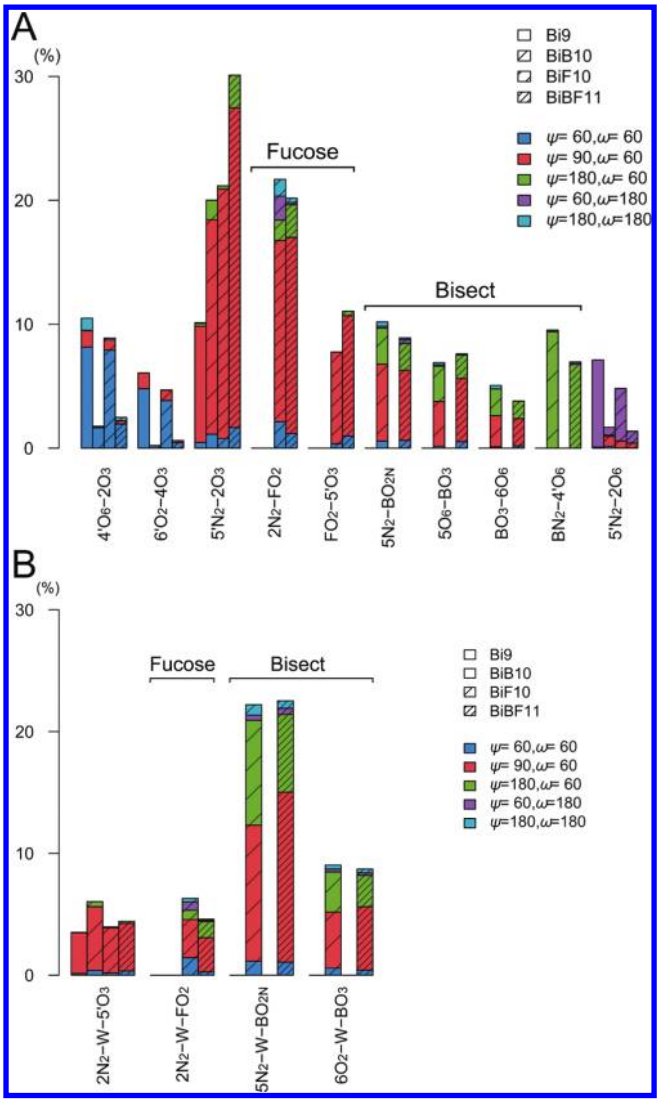

Figure 4. The probability distribution of (A) direct and (B) water mediated inter-residue H-bonds found in the simulations of the four N-glycans. Each color corresponds to a different conformation (blue: ψ/ω of 60°/60°, red: 90°/60°, green: 180°/60°, purple: 60°/180°, cyan: 180°/180°). Different types of bars are used to distinguish the four N-glycans. The labels indicate the donor/acceptor residue pairs (e.g., $4'O_6$–$2O_3$ represents the H-bond between the O_6 atom of residue 4′ (donor) and the O_3 atom of residue 2 (acceptor)).

folding of the α1,6-arm. The other three H-bonds form to a lesser extent, but their contributions are not negligible. The $2N_2\cdots W\cdots 5'O_3$ H-bond is found in all four N-glycans, indicating that water contributes to the back folding of the α1,6-arm.

In summary, the modifications strengthen the H-bonds that maintain the distinct conformers. This implies that the electrostatic contribution is at least as important as the steric effect in the N-glycan modifications. The same picture was obtained by Woods and co-workers from MD simulations of $Man_9GlcNAc_2$ in solution.[27]

Validation of Simulation Results. In order to assess the convergence of conformational sampling, we plotted the relative populations of each cluster (**a**, **b**, **c**, **a′**, and **c′**) as a function of simulation time for all four N-glycans (Figure S5, Supporting Information). The relative population size of each conformer drastically changes during the first 20 ns (1.3 μs in total) of simulation and reaches values close to those in Table 1

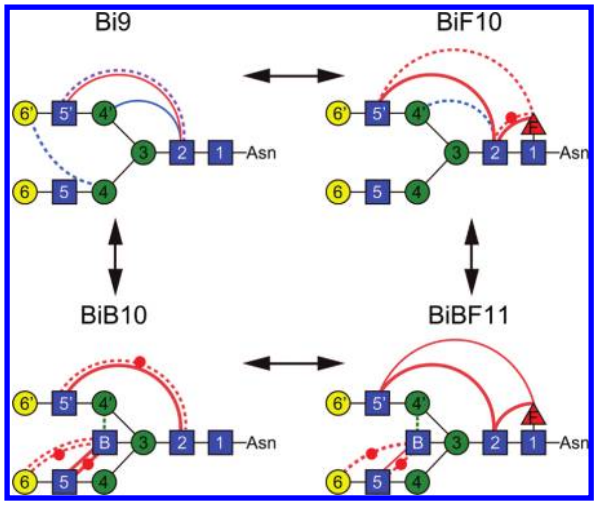

Figure 5. Schematic illustration of the inter-residue H-bond pattern. The same color definition as in Figure 4 was used to represent the type of H-bond. Different types of lines were used to indicate the probabilities of the H-bond (thick: ≥20%, solid: ≥10% (and <20%), dotted: ≥5% (and <10%)). The lines with a red circle indicate water mediated H-bonds.

at around 30 ns (1.9 μs in total). Convergence was achieved after approximately 40 ns (2.6 μs in total), assuring that our simulations sampled enough conformational space and the resultant populations of each cluster are well converged.

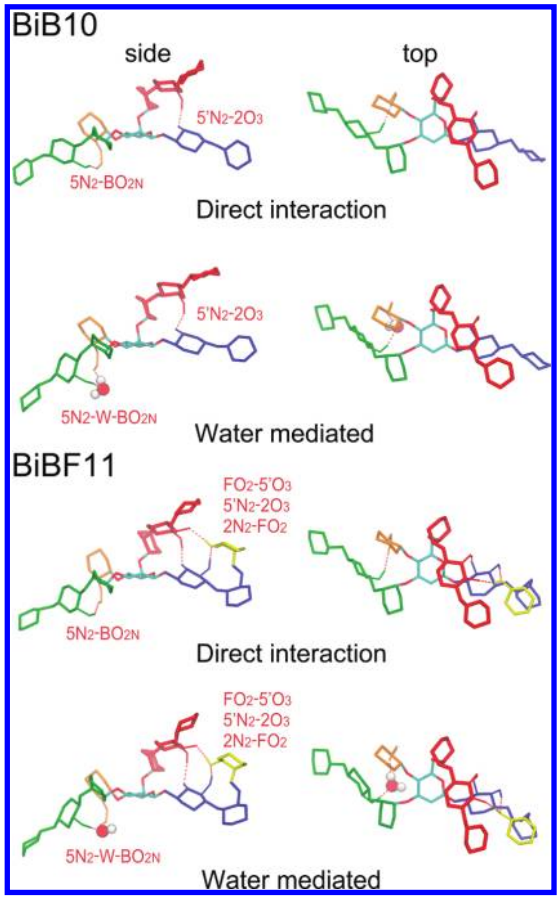

Figure 6. A typical snapshot for direct and water mediated H-bonds stabilizing the "backfold" conformation of BiB10 and BiBF11.

dx.doi.org/10.1021/jp212550z | J. Phys. Chem. B 2012, 116, 8504–8512

To quantitatively compare with available experimental data, NOE distances and scalar *J*-coupling constants, which are used to determine the glycosidic conformation, were calculated for Bi9 and BiBF11. Table 2 lists the average NOE distances for the Manα1-3Man linkage calculated from the present simulation. The corresponding experimental values are also shown in the same table.[14] The calculated distances are very close to the experimental values (the largest deviation being 0.63 Å for the 4-H1, 3-H2 pair in Bi9). NOE distances calculated for each cluster (**a**−**c**′) are almost identical to the average values in Table 2 due to the restricted conformational diversity of the α1,3-arm (see Figure 3E). Experimentally, the presence of 3-H2, 4-H5 NOE intensity only in BiBF11 has been attributed to a modification-induced conformational transition. In the unmodified N-glycan, Bi9, the simulation predicted the corresponding NOE distance to be 2.91 Å, which is slightly longer than that for BiBF11. Analysis of the trajectory shows that the fluctuation of the 3-H2···4-H5 inter-proton distance for Bi9 is twice that of BiBF11 (standard deviations of 0.77 and 0.44 Å for Bi9 and BiBF11, respectively). The longer inter-proton distance and greater fluctuation might explain the absence of NOE intensity in Bi9.

Table 2. Intra- and Inter-Residue NOE Distances (in Å) Calculated for Bi9 and BiBF11

		inter-proton distance (Å)	
conformation	NOE contact	MD simulation	experiment[a]
Bi9	4-H1, 4-H2	2.54	2.62
	4-H1, 3-H2	3.71	3.08
	4-H1, 3-H3/H4	2.34/4.08	2.07
	3-H2, 3-H1	2.45	2.53
	3-H2, 4-H1	3.71	3.00
BiBF11	4-H1, 4-H2	2.52	2.64
	4-H1, 3-H3	2.29	2.26
	3-H2, 3-H3	2.42	2.49
	3-H2, 4-H5	2.84	2.66

[a]Taken from ref 14.

Table 3 shows both the calculated and experimentally determined *J*-coupling constants (J_{56}, $H_5-C_5-C_6-H_6$; $J_{56'}$, $H_5-C_5-C_6-H_{6'}$)[15] for the Manα1-6Man linkage. Experimentally, two distinct values, 2.1 and 5.8 Hz, were obtained for Bi9, while a single value of ∼2 Hz was observed for BiBF11.[15] Our simulation well reproduces this tendency. The calculated *J* values for three clusters (gg, gt, and tg conformers) show that the difference between Bi9 and BiBF11 arises from the non-negligible contribution of gt conformers (MD population of 28%) for the former. The result agrees with the idea, derived originally from experiment, that Bi9 exists as a mixture of gg and gt conformers and that the introduction of bisecting GlcNAc and/or the core fucose reduces the diversity. The calculated values show large standard deviations possibly due to the significant conformational flexibility of the α1,6 linkage.

Table 3. Scalar ^3J-Coupling Constants (Hz) of the Manα1-6Man Structure Calculated for Bi9 and BiBF11[a]

	experiment[b]		MD simulation		
conformation	J_{56}	$J_{56'}$	J_{56}	$J_{56'}$	population
Bi9	2.1	5.8	2.8 (1.4)	4.4 (4.0)	
gauche−gauche (gg)			2.4 (1.0)	2.0 (1.3)	71%
gauche−trans (gt)			3.8 (1.5)	10.3 (1.6)	28%
trans−gauche (tg)			8.6 (2.3)	3.7 (2.3)	<1%
BiBF11	∼2	∼2	2.3 (1.0)	2.5 (2.2)	
gauche−gauche (gg)			2.3 (0.9)	2.0 (1.1)	94%
gauche−trans (gt)			3.6 (1.5)	10.2 (1.6)	6%
trans−gauche (tg)			6.7 (2.5)	4.1 (3.5)	<1%

[a]The standard deviation for each calculated value is shown in parentheses. [b]Taken from ref 15.

Comparison with Previous Structural Models. Previous structural models of N-glycan modifications have involved a conformational transition between two states, namely, "folded" and "extended" forms.[13−15,20,28] In Figure 7, we present our structural model based on the simulations, showing the effect of the two N-glycan modifications. First, our results show five distinct conformations of the N-glycan, each of which is characterized by the orientation of the α1,6-arm. The modifications reduce the conformational variety by shifting the equilibrium population of each conformer, rather than by generating a new, unique conformer.

Second, our model shows that the backfolding of the α1,6-arm (*swing* motion) can be attributed to the changes in the ψ angle, rather than the ω angle as previously thought.[13] The ω angle (gg and gt linkage orientations) provides another conformational variant (*up down* motion). Both the local solvation around the Manα1-6Man linkage[22] and the core modification can affect the relative population of each conformer. The *up down* motion can be analyzed in terms of scalar J_{HH} coupling along the C5−C6 bond (ω angle), as shown in the present study. Measurement of *J*-coupling on the ψ angle or NOE for the Manα1-6Man linkage could provide information about the *swing* motion ("folded/extended" transition).

Finally, the simulations show that the effect of bisecting GlcNAc on the N-glycan structure is greater than that of core fucose. On the basis of their NMR analysis, Homans et al. categorized type 2p and type 2d transitions as those in which the flexible region and the modification site are proximal or distal, respectively.[13] Using this definition, the introduction of bisecting GlcNAc corresponds to type 2p, and core fucosylation to type 2d. The former rearranges the inter-residue H-bond pattern directly involved in the conformational transition, significantly changing the conformational equilibria, whereas the core fucose directly interacts only with its neighbor or a residue near the branch end, only slightly shifting the conformational equilibria. In the actual glycoprotein, the core fucose is near the protein surface and their interactions must significantly change the overall structural orientation of the N-glycan. Simulation studies of oligosaccharides directly attached to glycoproteins will add further insights into the role of core fucosylaton, eventually providing a comprehensive molecular model for glycan−protein interactions.

■ CONCLUSIONS

We have performed REMD simulations of four N-glycan systems in explicit water to investigate the effect of the introduction of bisecting GlcNAc and core fucosylation. The simulations revealed five distinct conformers of the N-glycan. The introduction of bisecting GlcNAc and/or core fucosylation reduces the number of major conformers by shifting the conformational equilibria. Our simulations provide the structural basis for understanding the concept of "conformer selection" for glycan−protein interactions, which has been widely accepted by experimentalists. Such studies could be

dx.doi.org/10.1021/jp212550z | J. Phys. Chem. B 2012, 116, 8504−8512

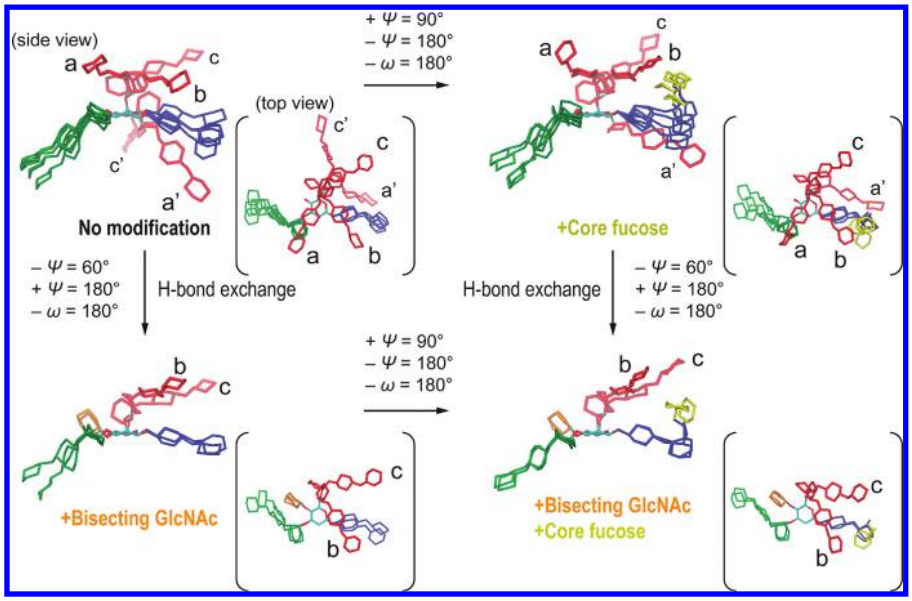

Figure 7. Structural model representing the effect of the introduction of bisecting GlcNAc and core fucosylation.

extended to simulations of N-glycans attached to glycoproteins based on enhanced conformational sampling methods like REMD. The free-energy analysis of glycoprotein simulation trajectories could yield fundamental principles for glycan–protein interactions that could be utilized in functional glycomics.

■ ASSOCIATED CONTENT

Ⓢ Supporting Information

Five figures relating to the performance of REMD simulations, RMSF of N-glycans, the relation between the local and global conformations, structures of distinct conformers of N-glycans, and the convergence of MD simulations are provided. This material is available free of charge via the Internet at http://pubs.acs.org.

■ AUTHOR INFORMATION

Corresponding Author

*E-mail: sugita@riken.jp (Y.S.); suyongre@riken.jp (S.R.).

Notes

The authors declare no competing financial interest.

■ ACKNOWLEDGMENTS

This research was supported in part by a Grant for Scientific Research on a Priority Area 'Transient macromolecular complex' (to Y.S.), the Development and Use of the Next-Generation Supercomputer Project of the Ministry of Education, Culture, Sports, Science and Technology (MEXT) (to Y.S.), the Fund for Seeds of Collaborative Research of the RIKEN (to Y.Y., Y.S., and S.R.), and the Fund from the High Performance Computing Infrastructure (HPCI) Strategic Program of MEXT (to Y.S.). We also thank the RIKEN Integrated Cluster of Clusters (RICC) for providing computational resources.

■ REFERENCES

(1) Imperiali, B.; O'Connor, S. E. *Curr. Opin. Chem. Biol.* **1999**, *3*, 643–649.
(2) Citri, A.; Yarden, Y. *Nat. Rev. Mol. Cell Biol.* **2006**, *7*, 505–516.
(3) Jefferis, R. *Trends Pharmacol. Sci.* **2009**, *30*, 356–362.
(4) Takahashi, M.; Kuroki, Y.; Ohtsubo, K.; Taniguchi, N. *Carbohydr. Res.* **2009**, *344*, 1387–1390.
(5) Zhao, Y. Y.; Sato, Y.; Isaji, T.; Fukuda, T.; Matsumoto, A.; Miyoshi, E.; Gu, J.; Taniguchi, N. *FEBS J.* **2008**, *275*, 1939–1948.
(6) Ferrara, C.; Grau, S.; Jäger, C.; Sondermann, P.; Brünker, P.; Waldhauer, I.; Hennig, M.; Ruf, A.; Rufer, A. C.; Stihle, M.; Umaña, P.; Benz, J. *Proc. Natl. Acad. Sci. U.S.A.* **2011**, *108*, 12669–12674.
(7) Hardy, B. J. *J. Mol. Struct.: THEOCHEM* **1997**, *395*, 187–200.
(8) Gabius, H. J.; André, S.; Jiménez-Barbero, J.; Romero, A.; Solís, D. *Trends Biochem. Sci.* **2011**, *36*, 298–313.
(9) Gabius, H. J. *Naturwissenschaften* **2000**, *87*, 108–121.
(10) Siebert, H. C.; André, S.; Lu, S. Y.; Frank, M.; Kaltner, H.; van Kuik, J. A.; Korchagina, E. Y.; Bovin, N.; Tajkhorshid, E.; Kaptein, R.; Vliegenthart, J. F. G.; von der Lieth, C. W.; Jiménez-Barbero, J.; Kopitz, J.; Gabius, H. J. *Biochemistry* **2003**, *42*, 14762–14773.
(11) Wormald, M. R.; Petrescu, A. J.; Pao, Y. L.; Glithero, A.; Elliott, T.; Dwek, R. A. *Chem. Rev.* **2002**, *102*, 371–386.
(12) Petrescu, A. J.; Petrescu, S. M.; Dwek, R. A.; Wormald, M. R. *Glycobiology* **1999**, *9*, 343–352.
(13) Homans, S. W.; Dwek, R. A.; Rademacher, T. W. *Biochemistry* **1987**, *26*, 6571–6578.
(14) Homans, S. W.; Dwek, R. A.; Rademacher, T. W. *Biochemistry* **1987**, *26*, 6553–6560.
(15) Homans, S. W.; Dwek, R. A.; Boyd, J.; Mahmoudian, M.; Richards, W. G.; Rademacher, T. W. *Biochemistry* **1986**, *25*, 6342–6350.
(16) Sayers, E. W.; Prestegaud, J. H. *Biophys. J.* **2000**, *79*, 3313–3329.
(17) Wooten, E. W.; Bazzo, R.; Edge, C. J.; Zamze, S.; Dwek, R. A.; Rademacher, T. W. *Eur. Biophys. J.* **1990**, *18*, 139–148.
(18) Barb, A. W.; Prestegard, J. H. *Nat. Chem. Biol.* **2011**, *7*, 147–153.
(19) Weller, C. T.; Lustbader, J.; Seshadri, K.; Brown, J. M.; Chadwick, C. A.; Kolthoff, C. E.; Ramnarain, S.; Pollak, S.; Canfield, R.; Homans, S. W. *Biochemistry* **1996**, *35*, 8815–8823.
(20) Stubbs, H. J.; Lih, J. J.; Gustafson, T. L.; Rice, K. G. *Biochemistry* **1996**, *35*, 937–947.
(21) Kim, H.; Choi, Y.; Lee, J.; Jeong, K.; Jung, S. *Bull. Kor. Chem. Soc.* **2009**, *30*, 2723–2728.
(22) Kirschner, K. N.; Woods, R. J. *Proc. Natl. Acad. Sci. U.S.A.* **2001**, *98*, 10541–10545.
(23) Almond, A. *Carbohydr. Res.* **2005**, *340*, 907–920.
(24) Perić-Hassler, L.; Hansen, H. S.; Baron, R.; Hünenberger, P. H. *Carbohydr. Res.* **2010**, *345*, 1781–1801.

(25) Corzana, F.; Motawia, M. S.; Du Penhoat, C. H.; Perez, S.; Tschampel, S. M.; Woods, R. J.; Engelsen, S. B. *J. Comput. Chem.* **2004**, *25*, 573−586.
(26) Naidoo, K. J.; Denysyk, D.; Brady, J. W. *Protein Eng.* **1997**, *10*, 1249−1261.
(27) Woods, R. J.; Pathiaseril, A.; Wormald, M. R.; Edge, C. J.; Dwek, R. A. *Eur. J. Biochem.* **1998**, *258*, 372−386.
(28) André, S.; Kožár, T.; Kojima, S.; Unverzagt, C.; Gabius, H. J. *Biol. Chem.* **2009**, *390*, 557−565.
(29) Salisburg, A. M.; Deline, A. L.; Lexa, K. W.; Shields, G. C.; Kirschner, K. N. *J. Comput. Chem.* **2009**, *30*, 910−921.
(30) Fernandes, C. L.; Sachett, L. G.; Pol-Fachin, L.; Verli, H. *Carbohydr. Res.* **2010**, *345*, 663−671.
(31) Mukhopadhyay, C. *Biopolymers* **1998**, *45*, 177−190.
(32) Sokolowski, T.; Peters, T.; Pérez, S.; Imberty, A. *J. Mol. Graphics Modell.* **1997**, *15*, 37−42.
(33) Balaji, P. V.; Qasba, P. K.; Rao, V. S. R. *Int. J. Biol. Macromol.* **1996**, *18*, 101−114.
(34) Qasba, P. K.; Balaji, P. V.; Rao, V. S. R. *J. Mol. Struct.: THEOCHEM* **1997**, *395*, 333−360.
(35) Sugita, Y.; Okamoto, Y. *Chem. Phys. Lett.* **1999**, *314*, 141−151.
(36) Re, S.; Miyashita, N.; Yamaguchi, Y.; Sugita, Y. *Biophys. J.* **2011**, *101*, L44−46.
(37) Miyashita, N.; Re, S.; Sugita, Y. Manuscript in preparation.
(38) Phillips, J. C.; Braun, R.; Wang, W.; Gumbart, J.; Tajkhorshid, E.; Villa, E.; Chipot, C.; Skeel, R. D.; Kale, L.; Schulten, K. *J. Comput. Chem.* **2005**, *26*, 1781−1802.
(39) Kirschner, K. N.; Yongye, A. B.; Tschampel, S. M.; González-Outeiriño, J.; Daniels, C. R.; Foley, B. L.; Woods, R. J. *J. Comput. Chem.* **2008**, *29*, 622−655.
(40) Jorgensen, W. L.; Chandrasekhar, J.; Madura, J. D.; Impey, R. W.; Klein, M. L. *J. Chem. Phys.* **1983**, *79*, 926−935.
(41) Woods, R. J. *GLYCAM Web*; Complex Carbohydrate Research Center, University of Georgia: Athens, GA, 2005−2011.
(42) Essmann, U.; Perera, L.; Berkowitz, M. L.; Darden, T.; Lee, H.; Pedersen, L. G. *J. Chem. Phys.* **1995**, *103*, 8577−8593.
(43) Haasnoot, C. A. G.; Deleeuw, F. A. A. M.; Altona, C. *Tetrahedron* **1980**, *36*, 2783−2792.
(44) DeMarco, M. L.; Woods, R. J. *Glycobiology* **2009**, *19*, 344−355.